AEROELASTIC AND STRUCTURES RESEARCH LABORATORY
MASSACHUSETTS INSTITUTE OF TECHNOLOGY

TECHNICAL REPORT 25-14

A STUDY OF THE STRUCTURAL DAMPING OF A SIMPLE BUILT-UP BEAM WITH RIVETED JOINTS IN BENDING

BY

T. H. H. PIAN

FOR THE

OFFICE OF NAVAL RESEARCH

CONTRACT N5ori-07833

ONR PROJECT NR064-259

MAY 1954

AEROELASTIC AND STRUCTURES RESEARCH LABORATORY

MASSACHUSETTS INSTITUTE OF TECHNOLOGY

TECHNICAL REPORT 25-14

A STUDY OF THE STRUCTURAL DAMPING OF A SIMPLE BUILT-UP BEAM WITH RIVETED JOINTS IN BENDING

FOR THE

OFFICE OF NAVAL RESEARCH

CONTRACT N5ori-07833

ONR PROJECT NR064-259

MAY 1954

Reported by: T. H. H. Pian

T. H. H. Pian

Approved by: R. L. Bisplinghoff

R. L. Bisplinghoff

ACKNOWLEDGEMENTS

The author wishes to acknowledge the assistance of Messrs. W. H. Campbell and G. S. Ram in the experimental phases of this investigation.

The manuscript of this report was edited by Mr. R. R. Staley and typed for reproduction by Mrs. S. Gleek. The figures were drawn by Messrs. C. Hanson and E. M. Zierhoffer.

TABLE OF CONTENTS

LIST OF ILLUSTRATIONS

ABSTRACT

A theory of structural damping in the bending of a simple built-up beam with either spliced joints or thin reinforcing spar caps is extended to include bending in which the screws or rivets block the sliding motion between the cap and the beam. The analysis assumes that the spar caps and the beam are held together by rivets which are distributed continuously and by pressures which depend upon the tightness of the rivet joint. The theoretical results indicate that, for beams with very flexible rivets, the energy loss per cycle is roughly inversely proportional to the tightness of the joint and tends to vary as the third power of the amplitude of vibration, provided the amplitude is not too large. For very small amplitudes, the same relationship holds for all rivets except very stiff ones. At the opposite extreme, the theory indicates that, for beams with very stiff rivets, the energy loss per cycle is directly proportional to the tightness of the joint and to the amplitude of vibration, provided that the amplitude is not too small. For very large amplitudes, this direct proportionality holds for all rivets except those which are very flexible.

Experimental measurements on a test beam provide a qualitative verification of the theory.

SECTION I

INTRODUCTION

In a previous paper (Ref. 1), the author made a theoretical study of the bending of a simple built-up beam with its reinforcing spar caps fastened by screws. This analysis assumes that the spar caps and the beam are held together by pressures which depend upon the tightness of the screw joints and that the screws in the holes have sufficient lateral clearance so as not to hinder any sliding motion between the cap and the beam. Thus, whenever the shear force between the two surfaces has reached the limiting friction force, a sliding motion begins, and the shear force is redistributed. The load-deflection relation and the energy loss per cycle of static loading were then determined. It was found that the non-linear component of the load-deflection curve contains mainly a second-power term and the energy loss per cycle varies approximately as the third power of the amplitude of vibration.

Reference 1 also describes an experimental investigation of the structural damping in built-up cantilever beams with spliced joints. It is shown that, for a beam with screw joints, the experimental results check quite favorably with the analytical solution, while for a built-up beam with tight-fit rivets, the results do not agree with the theory. It is the purpose of the present research program to extend the theory given in Reference 1 to the bending of built-up beams in which the screws or rivets block the sliding motion between the cap and the beam.

SECTION II

THEORETICAL ANALYSIS

2.1 Bending of a Riveted Built-Up Beam

The problem to be considered here is that of a cantilever beam with reinforcing spar caps, shown in Figure 1, subjected to a vertical shear load F at the free end.

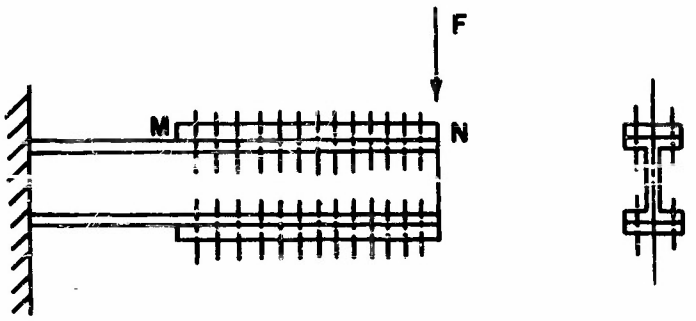

FIGURE 1 CANTILEVER BEAM WITH REINFORCING SPAR CAPS

The reinforcing cap is attached to the beam by rivets or by tightly fitted screws. The sliding motion between the cap and the beam is resisted by friction forces which depend upon the pressure between and the smoothness of the two surfaces and upon elastic forces which depend upon the shear rigidity of the rivets. To simplify the analysis, it is assumed that the rivets are so closely spaced that they can be replaced by a continuous shear joint. The shear deformation of the rivets varies linearly with the shearing force applied.

It is further assumed that the thickness of the caps is small in comparison to the depth of the beam so that the moment of inertia of the laminated section can be expressed by

$$I_{total} = I + \frac{1}{2} A h^2 \qquad (1)$$

where

I is the moment of inertia of the beam without the caps

A is the cross-sectional area of one cap

h is the depth of the beam.

Following the reasoning given in Reference 1, it is concluded that, for the given beam subjected to a shear force F, the shear force distribution along the plane MN between the cap and the beams may be divided into two regions (see Figure 2). In the region between M and P, the shear force is negative, and there is a sliding motion between the two surfaces. Beyond this region, no sliding motion occurs, and the shear distribution is the same as that of a solid beam.

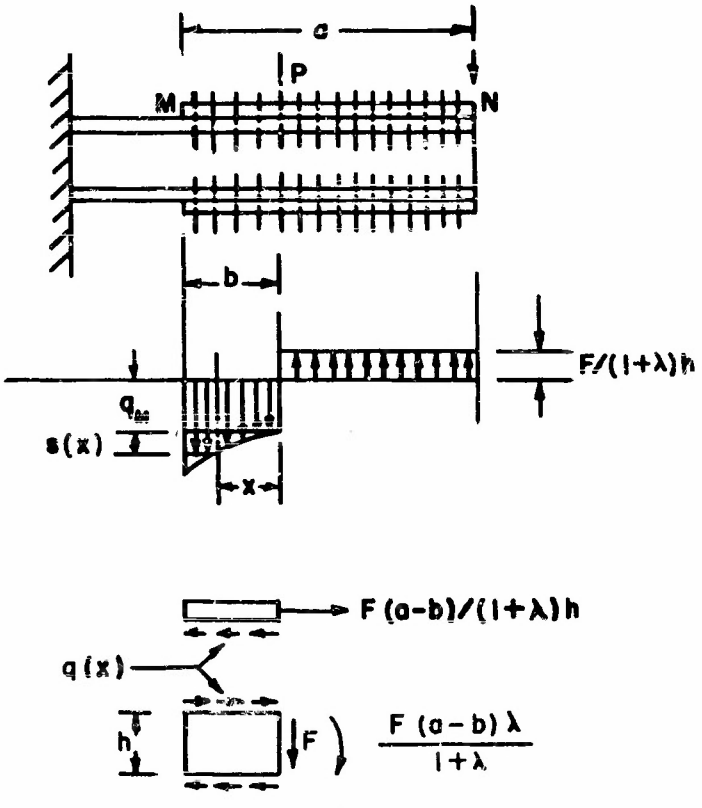

FIGURE 2 STRESS DISTRIBUTION ALONG THE JOINT

The shear force in the region PN can be determined by the elementary theory

$$q = FQ/I_{total} \qquad (2)$$

where Q is the static moment with respect to the neutral axis of the cross section of the spar cap. This is reduced to

$$q = F/(1+\lambda)h \tag{3}$$

where

$$\lambda = 2I/Ah^2 \tag{4}$$

The shear force in the region MP can be expressed by

$$q(x) = q_M + s(x) \tag{5}$$

where

q_M is the limiting shear force per unit length between the cap and the beam

$s(x)$ is the shear load in the continuous joint per unit length

x is the distance measured from the point P.

By considering the equilibrium condition of the segment MP of the spar cap, one obtains

$$\frac{F(a-b)}{(1+\lambda)h} = q_M b + \int_0^b s(x)\,dx \tag{6}$$

In the present case, the relative displacement between the spar cap and the beam, $r(x)$, is equal to the shear deformation of the joint at the point x. If k is the spring constant, defined by the distributed shear load per unit length required for a unit displacement, one obtains

$$r(x) = s(x)/k \tag{7}$$

The unknown function, $s(x)$, can be determined by the condition of consistency of deformation.

The elongation of the outer fiber for the length x of the beam can be written as

$$e(x) = \int_0^x \frac{Mh}{2EI}\, dx \tag{8}$$

where M is the bending moment. By substituting

$$M = \frac{F(a-b)\lambda}{1+\lambda} + Fx + q_M h x + h\int_0^x s(x)\, dx \tag{9}$$

in equation (8), one obtains

$$e(x) = \frac{h}{2EI}\left[\frac{F(a-b)\lambda}{1+\lambda}x + (F + q_M h)\frac{x^2}{2} + h\int_0^x\int_0^x s(x)\, dx\, dx\right] \tag{10}$$

The corresponding elongation of the spar cap is

$$e(x) = \int_0^x \sigma(x)\, dx \tag{11}$$

where $\sigma(x)$ is the normal stress in the spar cap. By substituting

$$\sigma(x) = \frac{1}{EA}\left[\frac{F(a-b)}{(1+\lambda)h} - q_M x - \int_0^x s(x)\, dx\right] \tag{12}$$

in equation (11), the following result is obtained

$$e(x) = \frac{1}{EA}\left[\frac{F(a-b)}{(1+\lambda)h}x - \frac{q_M x^2}{2} - \int_0^x\int_0^x s(x)\, dx\, dz\right] \tag{13}$$

The introduction of the condition that the elongation of the outer fiber is equal to the sum of the elongation of the spar cap and the joint deformation, obtained from equations (7), (10) and (13), yields

$$\frac{h}{2EI}\left[\left\{F + q_M h(1+\lambda)\right\}\frac{x^2}{2} + h(1+\lambda)\int_0^x\int_0^x s(x)\, dx\, dx\right] = \frac{s(x)}{A} \tag{14}$$

Differentiating equation (14) twice produces the following equivalent differential equation:

$$\frac{d^2 s}{dx^2} - \frac{k h^2 (1+\lambda)}{2EI} s = \frac{k h}{2EI}\left[F + q_M h (1+\lambda)\right] \qquad (15)$$

with the boundary conditions that

$$\text{at } x = 0, \qquad s = \frac{ds}{dx} = 0. \qquad (16)$$

The solution of equation (15) is

$$s(x) = q_M \left(\frac{1+\lambda+\phi}{1+\lambda}\right)\left[\cosh \frac{x}{\mu} - 1\right] \qquad (17)$$

where

$$\mu = \sqrt{\frac{2EI}{k h^2 (1+\lambda)}} \qquad (18)$$

$$\phi = F / q_M h . \qquad (19)$$

The substitution of equation (17) into (6) and solution for b, the region where the sliding motion occurs, give

$$b = \mu \sinh^{-1} \frac{\phi a}{(1+\lambda+\phi)\mu} \qquad (20)$$

In studying the damping characteristics of a built-up beam, it is necessary to determine the load-deflection characteristics of the beam. As in Reference 1, the additional deflections which result from the sliding motion between the cap and the beam are investigated. The only difference in the stress distribution between the solid and the built-up beam is the difference in the bending moment distribution within the segment MP. The additional moment at x of the built-up beam is

$$\Delta M(x) = \left[q_M + F/(1+\lambda)h\right] h x + h \int_0^x s(x)\, dx$$
$$= q_M h \left(\frac{1+\lambda+\phi}{1+\lambda}\right) \mu \sinh \frac{x}{\mu} \qquad (21)$$

Hence, the additional deflection at the tip of the built-up beam is

$$\Delta\delta = \frac{1}{EI}\left[(a-b)\int_0^b \Delta M(x)\,dx + \int_0^b\int_x^b \Delta M(x)\,dx\,dx\right]$$

$$= \frac{q_m h(1+\lambda+\phi)\mu^2}{EI(1+\lambda)}\left[a\cosh\frac{b}{\mu} - a + b - \mu\sinh\frac{b}{\mu}\right] \tag{22}$$

Substitution of the expression for b of equation (20) into equation (22) gives

$$\Delta\delta = \frac{q_m h(1+\lambda+\phi)\mu^2}{EI(1+\lambda)}\left[a\left\{\sqrt{\left[\frac{\phi a}{(1+\lambda+\phi)\mu}\right]^2+1} - \frac{1+\lambda+2\phi}{1+\lambda+\phi}\right\} + \mu\sinh^{-1}\frac{\phi a}{(1+\lambda+\phi)\mu}\right] \tag{23}$$

It should be remarked that the load-deflection relation derived above is limited to the case when there is no residual stress in the structure. During a process of cyclic loading, residual stress exists in the beam, and a different load-deflection relation will hold. By the same argument given in Reference 1, it can be shown that after the reproducible state has been reached in cyclic loading, the additional beam deflection resulting from the slippage of joint can again be expressed by equation (23) except that ϕ is now defined by

$$\phi = \Delta F / 2q_m h \tag{24}$$

where ΔF is the increase in shear load with respect to the lower load limit.

It can also be seen that for very large value of μ, i.e., for the case where the rivets offer very little resistance, equation (23) becomes

$$\Delta\delta \cong \frac{Fa^3\phi}{6EI(1+\lambda)(1+\lambda+\phi)^2}\left[3(1+\lambda)+2\phi\right] \tag{25}$$

This equation is equivalent to equation (31) of Reference 1.

2.2 Energy Loss per Cycle of Static Loading

The energy loss per cycle of static loading is equal to the area of the hysteresis loop of the load-deflection curve. This area is the same as the area of ΔF vs. $\Delta\delta$ curve, shown in Figure 3.

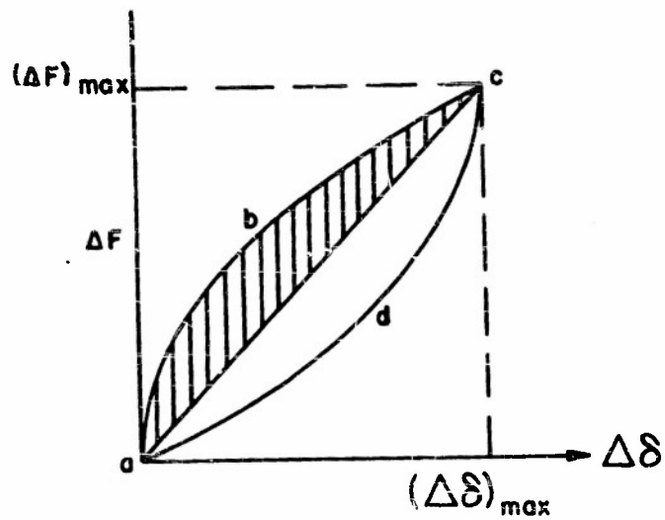

FIGURE 3 HYSTERESIS LOOP

In this figure, the curve abc is represented by equation (23). The energy loss per cycle of static loading is equal to the area enclosed by the curve $abcda$, which is equal to twice the shaded area shown in Figure 3. The shaded area can of course be expressed by

$$\frac{1}{2}(\Delta F)_{max}(\Delta\delta)_{max} - \int_0^{(\Delta F)_{max}} (\Delta\delta)\, d(\Delta F)$$

Thus, the energy loss per cycle is

$$\Delta W/\sim = (\Delta F)_{max}(\Delta\delta)_{max} - 2\int_0^{(\Delta F)_{max}} (\Delta\delta)\, d(\Delta F) \qquad (26)$$

By introducing the expression for $\Delta\delta$ in equation (23) and by substituting

$$\Delta F = 2 q_m h \phi$$

one obtains

$$\Delta W/\sim = \frac{4 q_m^2 h^2 \mu^3 (1+\lambda+\phi)}{\epsilon I} \left[\frac{\phi a}{(1+\lambda+\phi)\mu} - \sinh^{-1} \frac{\phi a}{(1+\lambda+\phi)\mu} \right] \tag{27}$$

It can be seen that for small values of ϕ/μ, i.e.,

$$\frac{\phi a}{(1+\lambda+\phi)\mu} - \sinh^{-1} \frac{\phi a}{(1+\lambda+\phi)\mu} \rightarrow \frac{1}{6} \left[\frac{\phi a}{(1+\lambda+\phi)\mu} \right]^3$$

equation (27) reduces to

$$\Delta W/\sim \simeq \frac{(\Delta F)^3 a^3}{12 \epsilon I q_m h (1+\lambda+\phi)^2} \tag{28}$$

which is equivalent to equation (55) of Reference 1. This indicates that, if the rivets of the built-up beam are very flexible and the amplitude is not too large, the energy loss per cycle varies approximately as the third power of the load amplitude and is roughly inversely proportional to the tightness of the joint. The same relationship holds for small amplitudes provided that the rivets are not too stiff.

For large values of ϕ/μ, $\sinh^{-1} \frac{\phi a}{(1+\lambda+\phi)\mu}$ become small compared with $\frac{\phi a}{(1+\lambda+\phi)\mu}$, and equation (27) then becomes

$$\Delta W/\sim \simeq \frac{2(\Delta F) q_m h \mu^2 a}{\epsilon I} \tag{29}$$

This shows that, if the rivets are very stiff and the amplitude of vibration is very large, the energy loss per cycle becomes proportional to both the load amplitude and the tightness of the joint. This relationship also holds if the amplitude is large, provided that the rivets are not too flexible.

SECTION III

EXPERIMENTAL INVESTIGATION

3.1 Description of the Tests

To verify the above theory, an experimental investigation of the effects of amplitude of load and of joint tightness on the energy loss in cyclic loading was carried out with a simple built-up beam. The test beam made of steel and had a cantilever support (see Figure 4). The cross section of the major part of the beam was I-shaped and reinforced on both sides by spar caps which were fastened with screws. It was expected that the sliding motion would occur in the first four inches from the inboard end of the reinforcing caps and special fasteners, shown in Detail A of Figure 4, were used in this region. The special fastener consisted of a long screw which had an appreciable flexibility to permit sliding motion between the cover plate and the beam. The nuts were set tightly with the plate and the beam; hence, the sliding motion between the two parts involved bending of the screws. The screw joint is used here in place of a rivet connection because there is no way to control the tightness and flexibility of rivets.

The stiffness of the individual fasteners was determined by using a pair of sliding blocks which were held together a single fastener as shown in Figure 5. A shear force was applied to the sliding block and the relation between the sliding motion and the applied force was determined. It was found that the stiffness of each screw varied between 16,700 lbs/ in and 12,500 lbs/ in with an average of 15,000 lbs/ in for various tightness of the screws. By refering to an equivalent joint of continuous properties, the stiffness, k , was 60,000 lbs/ in/in.

The limiting friction between the beam and the plate is a function of the tightness of the fastener and was determined by the torque required to slide the lap-joint specimen shown in Figure 6. The specimen with a different number of screws and different tightnesses were tested by a tensile testing machine under controlled rate of loading. It was found that the rate of loading had little effect on the limiting sliding friction which is directly proportional to the torque applied to the screws and approximately proportional to the number of screws. By referring to an equivalent joint of continuous properties, the limiting friction, q_m , was given by

$$q_m \text{ (in lbs/inch)} = 20 \times \text{(tightness of screw measured in torque of in-lbs.)}$$

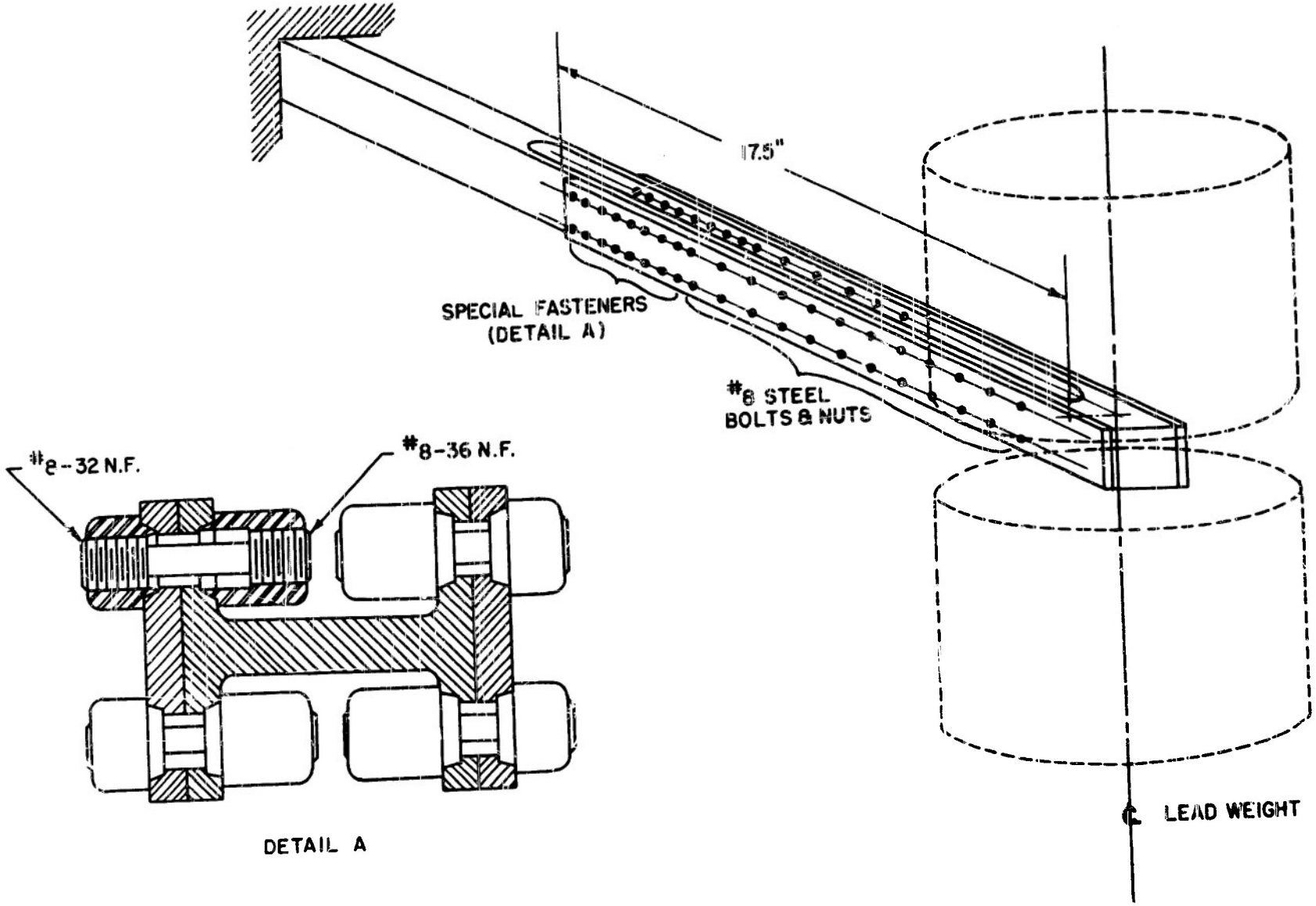

FIGURE 4 EXPERIMENTAL TEST SET-UP

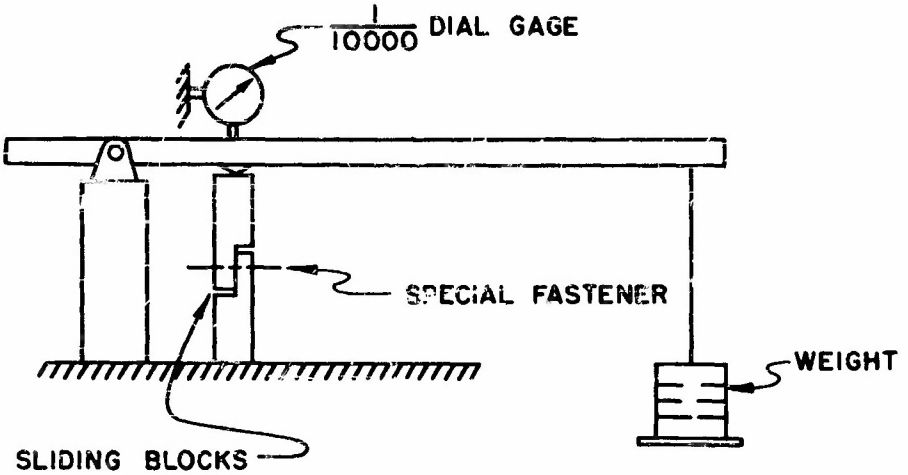

FIGURE 5 ARRANGEMENT FOR DETERMINATION OF SCREW STIFFNESS

The structural damping in terms of the loss of energy per cycle of vibration was measured by the rate of decay of free vibration, as was done in the previous investigation of Reference 1. A 60 pound lead mass was bolted to the free end of the beam. The beam was deflected to one side by string and then released by cutting the string. The decay of the beam was measured from a pair of electric strain gages mounted on opposite sides of the beam close to the root and their readings recorded on the Consolidated dynamic recording equipment. Methods for reducing the decay data to energy loss per cycle are given in Reference 1 and are also described briefly in Appendix A.

Tests were run under four different values of screw tightness: 2, 4, 6 and 8 in-lbs of torque. The equivalent values of limiting sliding friction q_M, are 40, 80, 120 and 160 lbs/in, respectively.

3.2 Results of Tests and Comparison with Theoretical Analysis

The results of the experimental investigation are presented by log-log plots of the energy loss per cycle against the double amplitude of the load at the end of

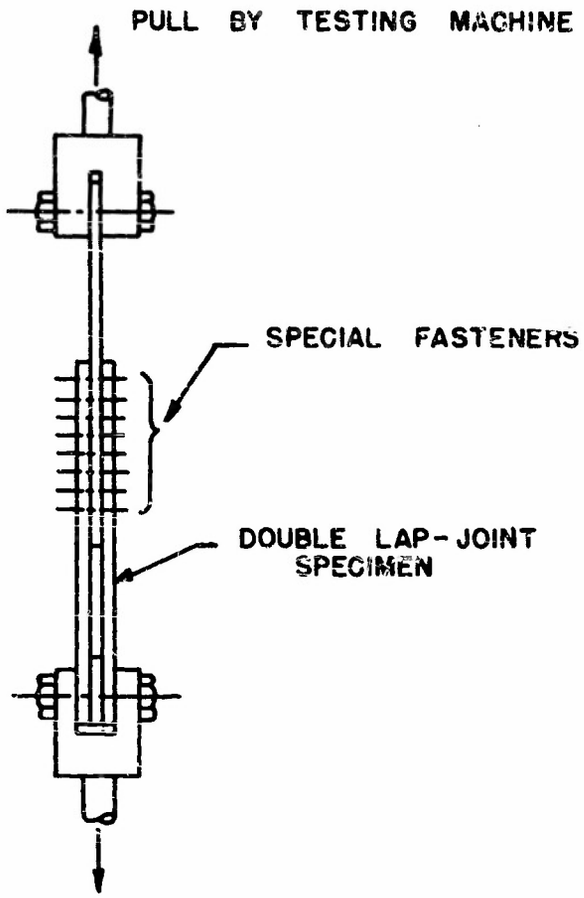

FIGURE 6 ARRANGEMENT FOR DETERMINATION OF LIMITING SLIDING FRICTION

the beam for four values of screw tightness (see Figure 7). For small amplitude of vibration the energy loss is approximately proportional to the third power of the amplitude, while for larger amplitude it is proportional to a lower power of the stress amplitude. This result agrees with the conclusion obtained by the theoretical analysis. Figure 7 also presents the theoretical solutions obtained from equation (27) for comparison. The pertinent data required for this analysis are given in Appendix A. Figure 7 shows that the experimental results are in qualitative

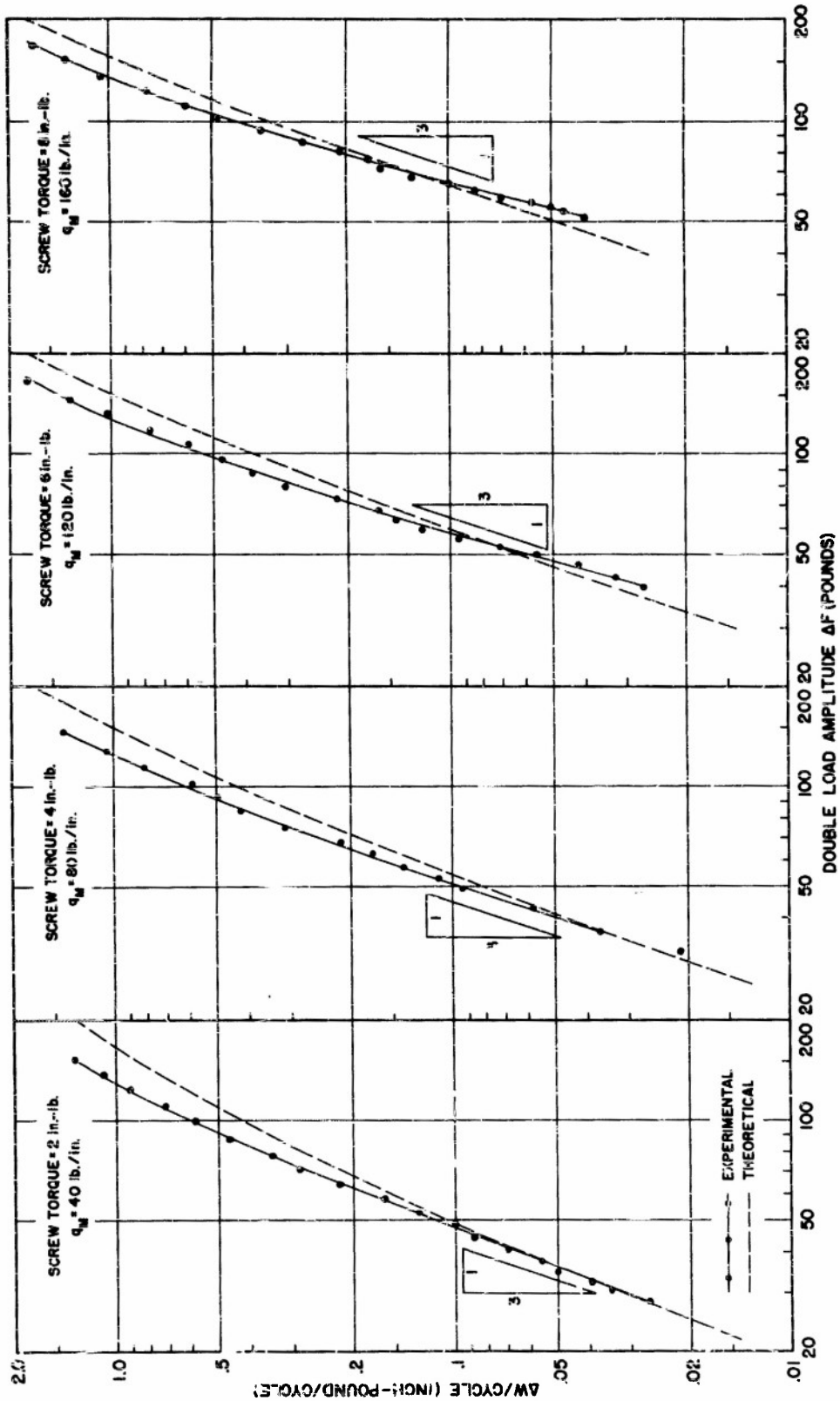

FIGURE 7 DAMPING IN BUILT-UP BEAMS

agreement with the theoretical solution. In all cases, the agreement between the two curves is fair at the lower amplitude region while the deviation becomes large at higher amplitudes.

The effect of the screw tightness on the structural damping is shown by re-drawing the test curves so as to produce the single plot of Figure 8. This figure reveals that, for low amplitude vibration, the energy loss is higher with lower screw tightness, while at high amplitudes, the effect of screw tightness on the energy loss becomes less important. In fact at very high amplitudes, the energy loss tends to become lower for lower screw tightness. This phenomenon has already been predicted by the theoretical analysis. The experimental and theoretical curves are plotted side by side in Figure 8 for comparison. The similarity of the two families of curves affords a qualitative proof of the above theory.

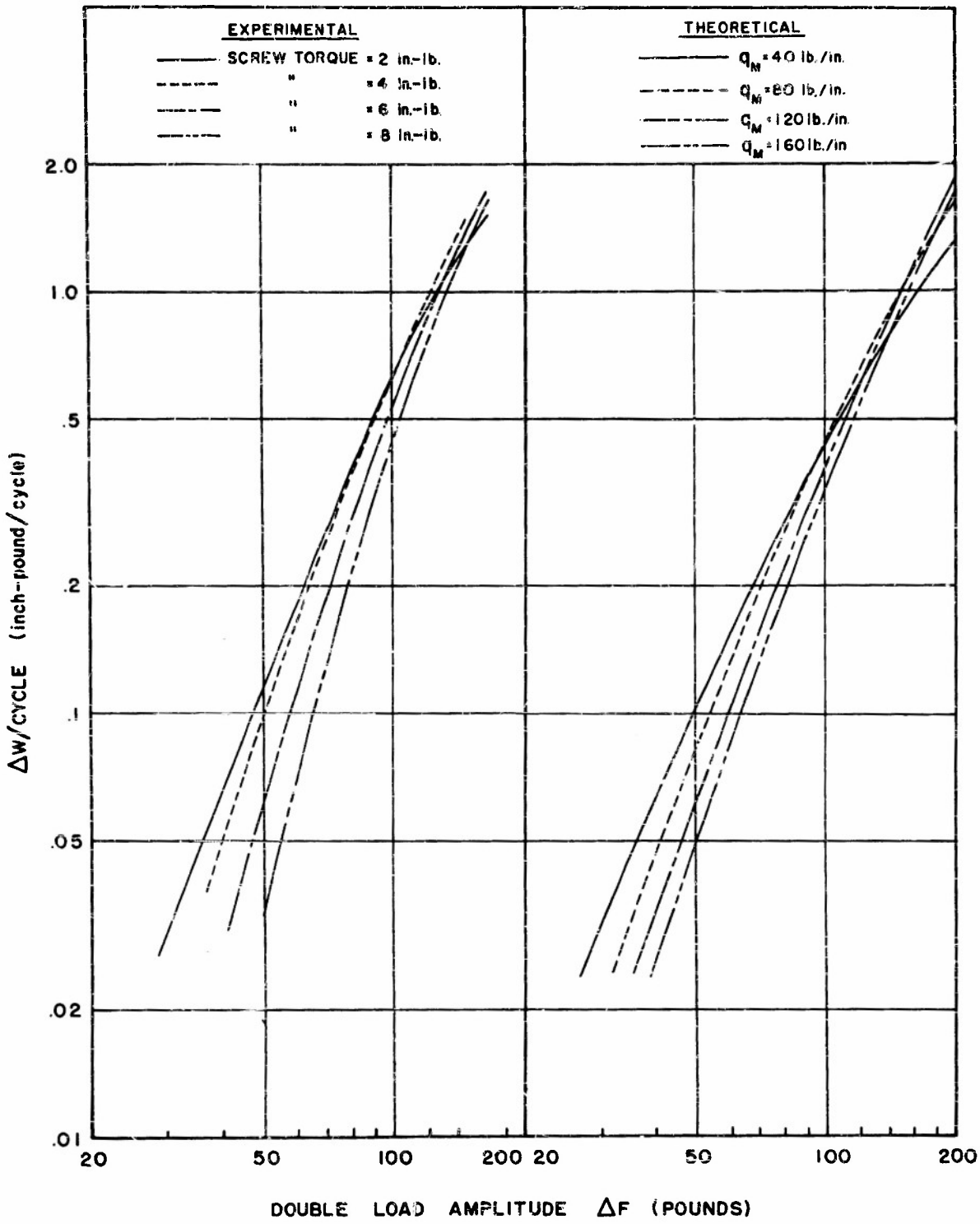

FIGURE 8 DAMPING IN BUILT—UP BEAMS

SECTION IV

CONCLUSIONS

An analytical expression has been obtained for the energy loss per cycle of vibration of a simple built-up beams with reinforcing spar caps fastened by rivets. The general trends as indicated by the theoretical expression are:

1. For beams with very flexible rivets, the energy loss per cycle is roughly inversely proportional to the tightness of the joint and approximately proportional to the third power of the amplitude of vibration, provided the amplitude is not too large. If the amplitude is restricted to very small values, the same relationship for the energy loss prevails for all rivets except those which are very stiff.

2. For beams with very stiff rivets, the energy loss per cycle is directly proportional to the tightness of the joint and the amplitude of vibration, provided that the amplitude is not too small. For very large values of the amplitude, this direct proportionality holds for all rivets except those which are very flexible.

The theoretical results have been verified qualitatively by experiments with a test beam with various joint tightnesses and amplitudes of vibration.

REFERENCES

1. Pian, T. H. H. and Hallowell, F. C., Jr. Investigation of Structural Damping in Simple Built-up Beams. Technical Report for Contract N5ori-07833 to ONR, by the Aeroelastic and Structures Research Laboratory, Massachusetts Institute of Technology, February 2, 1950. (A slightly condensed version is published in the Proceedings of the First U. S. National Congress of Applied Mechanics, June 11-16, 1951 pp. 97-102.)

APPENDIX A

REMARKS ON COMPUTATIONS

(1) Calculation of Energy Loss per Cycle from Decay Curve

In the equivalent viscous damping method of Reference 1, the energy loss per cycle is given by

$$\Delta W/\sim = K A_{n+\frac{1}{2}}^2 \ell_n \left(\frac{x_n}{x_{n+1}}\right)$$

where

K is the stiffness of the beam

$A_{n+\frac{1}{2}}$ is the amplitude of vibration of the tip mass at the $n+\frac{1}{2}$ cycle

x_n is the amplitude of the n^{th} cycle of vibration as shown by the oscillograph record.

The amplitude, $A_{n+\frac{1}{2}}$, is related to $x_{n+\frac{1}{2}}$ through a calibration constant which depends on the location of the strain gages and the attenuation of the recording system.

(2) Theoretical Relations between the Energy Loss per Cycle and the Limiting Friction and the Load Amplitude

The theoretical relation is given by equation (27),

$$\Delta W/\sim = \frac{4 q_m^2 h^2 \mu^3 (1+\lambda+\phi)}{EI}\left[\frac{\phi a}{(1+\lambda+\phi)\mu} - \sinh\frac{-1\ \phi a}{(1+\lambda+\phi)\mu}\right]$$

where

q_m is the limiting sliding friction in lbs/in

h is the depth of the I-beam = 1"

E is Young's modulus = 30×10^6 p.s.i.

I is the moment of inertia of the I-beam = 0.0545 in^4

a is the length of reinforcing cap = 17.5 in

$$\mu = \sqrt{\frac{2EI}{k h^2 (1+\lambda)}}$$

k is the stiffness of the screw = 60,000 lb./in/in

$$\lambda = \frac{I}{\frac{1}{2} A h^2}$$

A is the cross-sectional area of the spar cap

$$\phi = \Delta F / 2 q_M h$$

ΔF is the double load amplitude.

The dimensions of the beam are given in Figure 9.

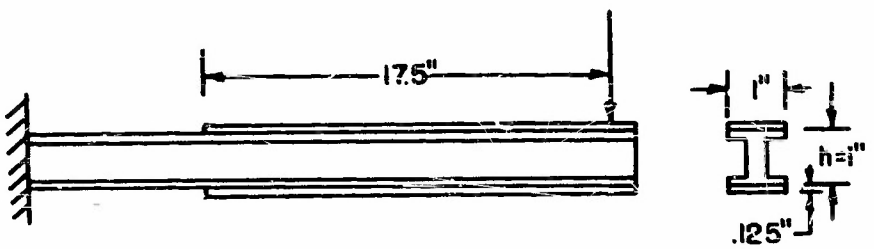

FIGURE 9 DIMENSIONS OF TEST BEAM

From the given data, the following results are obtained:

$\lambda = 0.872$

$\mu = 5.4$ in

$$\Delta W/\sim = (3.85 \times 10^{-4})\, q_M^2 (1.872+\phi)\left[\frac{\phi}{3.24(1.872+\phi)} - \sinh^{-1}\frac{\phi}{3.24(1.872+\phi)}\right] \qquad \text{(A.1)}$$

and $$\Delta F = 2 q_M \phi. \qquad \text{(A.2)}$$

Then, from equations (A.1) and (A.2) the relation between $\Delta W/\sim$ and ΔF can be calculated for any given value of limiting sliding friction, q_M.

DISTRIBUTION LIST

Technical Reports

Contract NR 064-259 Project NR 064-259

Chief of Naval Research
Department of the Navy
Washington 25, D.C.
Attn: Code 438 (2)

Director,
Office of Naval Research
Branch Office
150 Causeway St.
Boston 14, Mass. (2)

Chief of Bureau of Aeronautics
Navy Department
Washington 25, D.C.
Attn: TD-41, Technical Library (1)
: DE-22, C. W. Hurley (2)

Chief of Bureau of Ordnance
Navy Department
Washington 25, D.C.
Attn: Ad-3, Technical Library (1)
: Re9a (1)

Chief of Bureau of Ships
Navy Department
Washington 25, D.C.
Attn: Director of Research (1)
: Code 442 (1)

Chief of Bureau of Yards and Docks
Navy Department
Washington 25, D.C.
Attn: Research Division (2)

Librarian
U. S. Naval Postgraduate School
Monterey, California (1)

Naval Air Experimental Station
Naval Air Material Center
Naval Base
Philadelphia 12, Pa.
Attn: Head, Aeronautical Materials Laboratory (1)

Naval Ordnance Laboratory
Naval Gun Factory
Washington 25, D.C.
Attn: Dr. D. E. Marlowe (1)

Superintendent
Naval Gun Factory
Washington 25, D.C. (1)

Naval Ordnance Test Station
Inyokern, California
Attn: Scientific Officer (1)

Director
David Taylor Model Basin
Washington 7, D.C.
Attn: Structural Mechanics Division (2)

Director
Naval Engineering Experiment Station
Annapolis, Maryland (1)

Director
Materials Laboratory
New York Naval Shipyard
Brooklyn 1, New York (1)

Chief of Staff
Department of the Army
The Pentagon
Washington 25, D.C.
Attn: Director of Research and Development (1)

Office of Chief of Ordnance
Research and Development Service
Department of the Army
The Pentagon
Washington 25, D.C.
Attn: ORDTB (1)

Commanding Officer
Watertown Arsenal
Watertown, Massachusetts
Attn: Laboratory Division (1)

Commanding Officer
Frankford Arsenal
Philadelphia, Pa.
Attn: Laboratory Division (1)

Commanding Officer
Squier Signal Laboratory
Fort Monmouth, New Jersey
Attn: Components and Materials Branch (1)

Commanding General
Air Materiel Command
Wright-Patterson Air Force Base
Dayton, Ohio
Attn: E. H. Schwartz - MCREXA-8 (3)

Director
National Bureau of Standards
Washington, D.C.
Attn: Dr. W. H. Ramberg (1)

U. S. Coast Guard
1300 E Street, NW
Washington, D.C.
Attn: Chief, Testing and Development Division (1)

Forest Products Laboratory
Madison, Wisconsin
Attn: L. J. Markwardt (1)

National Advisory Committee for Aeronautics
1724 F Street, NW
Washington, D.C.
Attn: Materials Research Coordination Group (2)

National Advisory Committee for Aeronautics
Langley Field, Virginia
Attn: Mr. E. Lundquist (1)
: Dr. Bernard Budiansky (1)

National Advisory Committee for Aeronautics
Cleveland Municipal Airport
Cleveland, Ohio
Attn: J. H. Collins, Jr. (1)

U. S. Maritime Commission
Technical Bureau
Washington, D.C.
Attn: Mr. Wenless (1)

Research and Development Board
Pentagon Building
Washington, D.C.
Attn: Library 3D641 (1)

Dr. S. P. Timoshenko
School of Engineering
Stanford University
Stanford, California (1)

Dr. D. C. Drucker
Graduate Division of Applied Mathematics
Brown University
Providence, Rhode Island (1)

Dr. J. E. Dorn
University of California
Berkeley, California (1)

Dr. T. J. Dolan
University of Illinois
Urbana, Illinois (1)

Professor R. L. Bisplinghoff
Massachusetts Institute of Technology
Cambridge 39, Massachusetts (15)

Dr. N. J. Hoff
Department of Aeronautical Engineering and Applied Mechanics
Polytechnic Institute of Brooklyn
99 Livingston Street
Brooklyn, New York (1)

Dr. N. M. Newmark
Department of Civil Engineering
University of Illinois
Urbana, Illinois (1)

Dr. J. N. Goodier
School of Engineering
Stanford University
Stanford, California (1)

Professor F. K. Teichmann
Department of Aeronautical Engineering
New York University
University Heights, Bronx
New York City, New York (1)

Professor Jesse Ormondroyd
University of Michigan
Ann Arbor, Michigan (1)

Dr. W. H. Hoppmann
Department of Applied Mechanics
Johns Hopkins University
Baltimore, Maryland (1)

Professor W. K. Krefeld
College of Engineering
Columbia University
New York, New York (1)

Professor R. M. Hermes
University of Santa Clara
Santa Clara, California (1)

Commanding Officer
Office of Naval Research
Branch Office
346 Broadway
New York 13, New York (1)

Commanding Officer
Office of Naval Research
Branch Office
844 N. Rush Street
Chicago 11, Illinois (1)

Commanding Officer
Office of Naval Research
Branch Office
1000 Geary Street
San Francisco 9, California (1)

Commanding Officer
Office of Naval Research
Branch Office
1030 Green Street
Pasadena, California (1)

Contract Administrator, SE Area
Office of Naval Research
Department of Navy
Washington 25, D.C.
Attn: Mr. R. F. Lynch (1)

Director, Naval Research Laboratory
Washington 20, D.C.
Attn: Technical Information Officer (9)
: Technical Library (1)
: Mechanics Division (2)

Dr. A. C. Eringen
Purdue University
Lafayette, Indiana (1)

Dr. M. Hetenyi
Northwestern University
Evanston, Illinois (1)

Officer In Charge
Office of Naval Research
Branch Office
Navy #100
Fleet Post Office
New York, New York (5)

Dr. C. B. Smith
College of Arts and Sciences
Department of Mathematics
Walker Hall
University of Florida
Gainesville, Florida (1)

Professor R. D. Mindlin
Department of Civil Engineering
Columbia University
Broadway at 117th Street
New York 27, New York (1)

Professor H. Bleich
Department of Civil Engineering
Columbia University
Broadway at 117th Street
New York 27, New York (1)

Mr. Martin Goland
4049 Pennsylvania Avenue
Midwest Research Institute
Kansas City 2, Missouri (1)

Professor George H. Lee
Department of Mechanics
Rensselaer Polytechnic Institute
Troy, New York (1)

Commander
U. S. Naval Proving Grounds
Dahlgren, Virginia (1)

Naval Ordnance Laboratory
White Oak, Maryland
RFD 1, Silver Spring, Maryland
Attn: Dr. C. A. Truesdell (1)

Director of Research and Development
Headquarters, U. S. Air Force
AFOED-RE-3
Washington 25, D. C. (1)

Professor W. Flugge
School of Engineering
Stanford University
Stanford, California (1)

Professor A. S. Veletsos
Department of Civil Engineering
University of Illinois
Urbana, Illinois (1)